IMPROVED CONSTRAINTS ON PRIMORDIAL NON-GAUSSIANITY FOR THE WILKINSON MICROWAVE ANISOTROPY PROBE 5-YR DATA

A. Curto[1], E. Martínez-González and R. B. Barreiro

IFCA, CSIC-Univ. de Cantabria, Avda. los Castros, s/n, E-39005-Santander, Spain

Draft version October 19, 2009

ABSTRACT

We present constraints on the non-linear coupling parameter f_{nl} with the Wilkinson Microwave Anisotropy Probe (WMAP) data. We use an updated method based on the spherical Mexican hat wavelet (SMHW) which provides improved constraints on the f_{nl} parameter. This paper is a continuation of a previous work by Curto et al. where several third order statistics based on the SMHW were considered. In this paper, we use all the possible third order statistics computed from the wavelet coefficient maps evaluated at 12 angular scales. The scales are logarithmically distributed from 6.9 arcmin to 500 arcmin. Our analysis indicates that f_{nl} is constrained to $-18 < f_{nl} < +80$ at 95% confidence level (CL) for the combined V+W WMAP map. This value has been corrected by the presence of undetected point sources, which adds a positive contribution of $\Delta f_{nl} = 6 \pm 5$. Our result excludes at $\sim$99% CL the best-fitting value $f_{nl} = 87$ reported by Yadav & Wandelt. We have also constrained f_{nl} for the Q, V and W frequency bands separately, finding compatibility with zero at 95 % CL for the Q and V bands but not for the W band. We have performed some further tests to understand the cause of this deviation which indicate that systematics associated to the W radiometers could be responsible for this result. Finally we have performed a Galactic North-South analysis for f_{nl}. We have not found any asymmetry, i.e. the best-fitting f_{nl} for the northern pixels is compatible with the best-fitting f_{nl} for the southern pixels.

Subject headings: methods: data analysis – cosmic microwave background

1. INTRODUCTION

The cosmic microwave background (CMB) offers a picture of the early Universe when it was only 400,000 years old. The CMB photons last scattered off electrons at that time and since then they traveled free through the space. The primordial perturbations set up during inflation are imprinted in both radiation and matter distribution. The CMB temperature anisotropies, related with the primordial perturbations, can be used to test some assumptions of the so called standard model. In particular, we can test the prediction of the standard, single field, slow roll inflation (Guth 1981; Albrecht & Steinhardt 1982; Linde 1982, 1983) which states that the anisotropies are compatible with a nearly Gaussian random field. Other non-standard models of inflation predict detectable levels of non-Gaussianity in the anisotropies (see e.g. Bartolo et al. 2004).

Primordial non-Gaussianity of the local form is characterised by the non-linear coupling parameter f_{nl} (Salopek & Bond 1990; Gangui et al. 1994; Verde et al. 2000; Komatsu & Spergel 2001):

$$\Phi(\mathbf{x}) = \Phi_L(\mathbf{x}) + f_{nl}\{\Phi_L^2(\mathbf{x}) - \langle\Phi_L^2(\mathbf{x})\rangle\} \tag{1}$$

where $\Phi(\mathbf{x})$ is the primordial gravitational potential and $\Phi_L(\mathbf{x})$ is a linear random field which is Gaussian distributed and has zero mean.

There are many studies based on different statistical tools to constrain the local f_{nl} parameter from the CMB anisotropies, using the data of different experiments. We can mention the analyses using the angular bispectrum and wavelets on the Cosmic Background Explorer (COBE) data (Komatsu et al. 2002; Cayón et al. 2003), the angular bispectrum on MAXIMA data (Santos et al. 2003), the angular bispectrum on WMAP data (Komatsu et al. 2003; Creminelli et al. 2006, 2007; Spergel et al. 2007; Yadav & Wandelt 2008; Komatsu et al. 2009; Smith et al. 2009), different kind of wavelet analyses on WMAP data (Mukherjee & Wang 2004; Cabella et al. 2005; Curto et al. 2009), the Minkowski functionals on BOOMERanG data (De Troia et al. 2007), the Minkowski functionals on Archeops data (Curto et al. 2007, 2008), the Minkowski functionals on WMAP data (Komatsu et al. 2003; Spergel et al. 2007; Gott et al. 2007; Hikage et al. 2008; Komatsu et al. 2009) among others. We can also mention new promising techniques as for example one based on the n-point probability density distribution (Vielva & Sanz 2009), and other based on needlets (Pietrobon et al. 2009; Rudjord et al. 2009). Other works are based on the use of the large scale structure to constrain f_{nl} (Slosar et al. 2008).

This work is a continuation of the wavelet-based analysis by Curto et al. (2009) of the WMAP[2] data. We use high resolution WMAP data maps, and compute the wavelet coefficients for 12 angular scales logarithmically spaced from 6.9 arcmin to 500 arcmin. With these wavelet coefficients we compute all the possible third order moments involving these scales.

The article is organised as follows. Section 2 presents the estimators used to test Gaussianity and to constrain f_{nl}, the data maps and the simulations. Section 3 summarises the main results of this work and the conclusions

---

Electronic address: curto@ifca.unican.es

[1] Also at Dpto. de Física Moderna, Univ. de Cantabria, Avda. los Castros, s/n, 39005-Santander, Spain

[2] http://map.gsfc.nasa.gov/

are in Section 4.

2. METHODOLOGY

This analysis is based on the spherical Mexican hat wavelet (SMHW) as defined in Martínez-González et al. (2002). For references about the use of the SMHW to test Gaussianity in the CMB see for example the review by Martínez-González (2008). We compute the wavelet coefficient maps at several scales R_i logarithmically separated (R_{i+1}/R_i constant). The considered scales are[3]: $R_1 = 6.9'$, $R_2 = 10.6'$, $R_3 = 16.3'$, $R_4 = 24.9'$, $R_5 = 38.3'$, $R_6 = 58.7'$, $R_7 = 90.1'$, $R_8 = 138.3'$, $R_9 = 212.3'$, $R_{10} = 325.8'$, $R_{11} = 500'$. We also include the unconvolved map, which will be represented by the scale R_0 as in Curto et al. (2009). For each possible combination of three scales R_i, R_j, and R_k (where the indices i, j, and k can be repeated) we define a third order statistic

$$q_{ijk} = \frac{1}{N_{i,j,k}} \sum_{p=0}^{N_{pix}-1} \frac{w_{p,i} w_{p,j} w_{p,k}}{\sigma_i \sigma_j \sigma_k} \qquad (2)$$

where N_{pix} is the total number of pixels of the map, $N_{i,j,k}$ is the number of pixels available after combining the extended masks corresponding to the three scales R_i, R_j and R_k, $w_{p,i} = w_p(R_i)$ is the wavelet coefficient in the pixel p evaluated at the scale R_i, and σ_i is the dispersion of $w_{p,i}$. Each map $w_{p,i}$ is masked out with the corresponding extended mask at the scale R_i as in Curto et al. (2009). For a set of n scales we have $n_{stat} = (n + 3 - 1)!/[3!(n - 1)!]$ third order statistics such as the one defined in Eq. (2). We have tested with simulations that these statistics have a Gaussian-like distribution. We can construct a vector $\mathbf{q}$ of dimension n_{stat}

$$\mathbf{q} = [q_{0,0,0}; q_{0,0,1}; ...; q_{0,0,11}; q_{0,1,1}; ...; q_{11,11,11}]. \qquad (3)$$

With this vector we can perform two different analyses using a χ^2 statistic: one to test Gaussianity and a second one to constrain f_{nl} (Eqs. (7) and (8) of Curto et al. 2009).

We use the 5-yr WMAP foreground reduced data, available in the Legacy Archive for Microwave Background Data Analysis (LAMBDA) web site[4]. We combine the maps of different radiometers using the inverse of the noise variance as an optimal weight (Bennett et al. 2003). In particular we analyse the V+W, Q, V and W combined maps at a resolution of 6.9 arcmin, corresponding to a HEALPix (Górski et al. 2005) $N_{side} = 512$. We use the $KQ75$ mask and also a set of extended masks for the wavelet coefficient maps. We use the same masks as the ones described in Curto et al. (2009) for a threshold of 0.01. This corresponds to an available fraction of the sky from 71.2% for the R_1 scale to 31.4% for the R_{11} scale. Notice that larger scales have the restriction of a lower available area, which means a lower sensitivity to f_{nl}.

Finally we analyse the data and compare them with Gaussian and non-Gaussian simulations. The Gaussian

[3] The level of discretisation of the wavelet space is a balance between the minimum number of scales needed to extract the non-Gaussian signal from the data and acceptable computational requirements.
[4] http://lambda.gsfc.nasa.gov

Map	χ^2_{data}	DOF	$\langle \chi^2 \rangle$	σ	$P(\chi^2 \leq \chi^2_{data})$
V+W	349	364	379	49.2	0.29
Q	384	364	378	48.7	0.63
V	348	364	377	47.8	0.27
W	354	364	376	47.9	0.35

Map	best f_{nl}	$\langle f_{nl} \rangle$	$\sigma(f_{nl})$	$X_{0.160}$	$X_{0.840}$	$X_{0.025}$	$X_{0.975}$
V+W	39	-1	25	-26	24	-51	47
Q	11	0	33	-31	34	-63	66
V	23	0	30	-28	30	-55	59
W	65	-4	30	-33	26	-59	58

simulations are performed using the best fit power spectrum C_ℓ for WMAP provided by LAMBDA and the instrumental white noise of each WMAP radiometer. The non-Gaussian simulations with the f_{nl} contribution are computed following the algorithms described in Liguori et al. (2003, 2007) and transformed into WMAP maps with the instrumental noise included. We also estimate the unresolved point source contribution to f_{nl} for the V+W case by analysing point source simulations. These simulations have been generated as in Curto et al. (2009) following the source number counts dN/dS given by de Zotti et al. (2005).

3. RESULTS

In this Section we present the Gaussianity analysis of the WMAP data for the combined V+W, Q, V, and W data maps. We also constrain f_{nl} for these maps through a χ^2 test. We estimate the contribution of point sources to the V+W map. Finally we constrain f_{nl} for northern and southern pixels separately.

3.1. *Analysis of WMAP data*

We evaluate the wavelet coefficients at the 12 considered scales. With these coefficients we compute the third order estimators defined in Eq. (2). For 12 scales, we have 364 possible third order statistics. We compute these statistics for the data maps and for Gaussian simulations. The covariance matrix used in the χ^2 statistics is constructed from 10,000 Gaussian simulations. For the considered cases, V+W, Q, V and W, we have that the data are inside the 2σ error bars, i.e., the data are compatible with Gaussian simulations. We compute a χ^2 statistic by comparing the data with the expected value of Gaussian simulations following Curto et al. (2009). We as well compute the χ^2 of an additional set of 1,000 Gaussian simulations. The χ^2 statistic of the data is compatible with the χ^2 of the Gaussian simulations. This is presented in Table 1.

We have studied the properties of the covariance matrix for the V+W map (see left panel of Fig. 1) which is
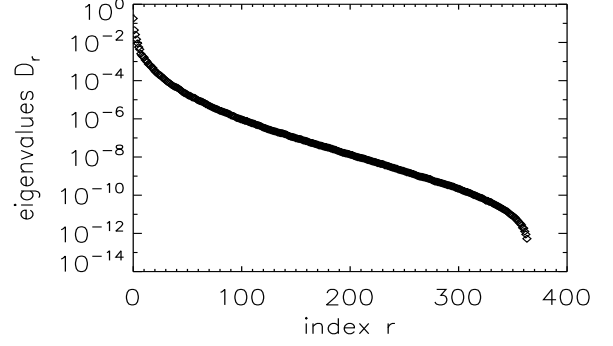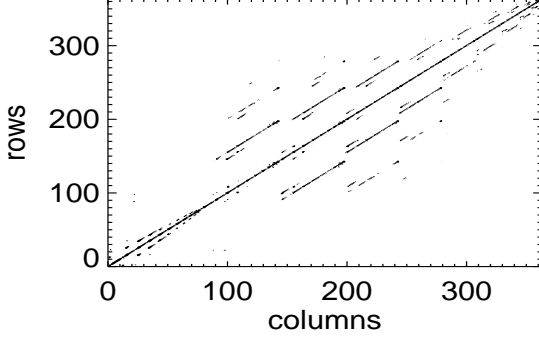
FIG. 1.— Left panel: the covariance matrix elements of the third order statistics for the V+W map that satisfy $C_{ijk,rst}/\sqrt{C_{ijk,ijk}C_{rst,rst}} > 0.95$. Right panel: the covariance matrix eigenvalues for the V+W map.
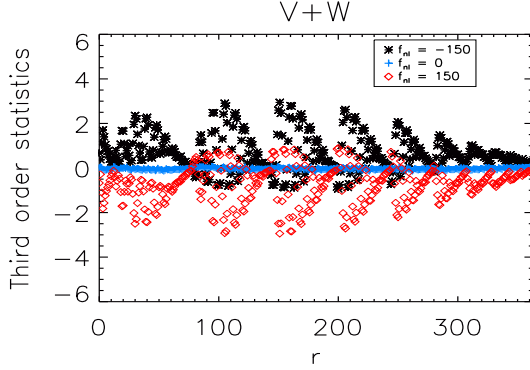

FIG. 2.— The expected values of the normalised third order statistics q_r for V+W simulations with different values of f_{nl}, where $r \equiv \{i,j,k\}$ is ordered following Eq. (3).
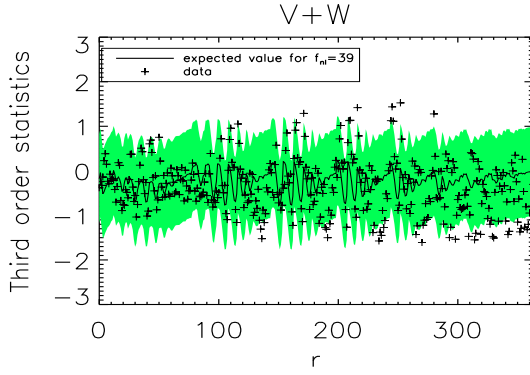

FIG. 3.— The normalised third order statistics q_r for the combined V+W data map. The solid line corresponds to the expected values for the best-fitting f_{nl} model ($f_{nl} = 39$). We also plot the 1σ error bars in green.

derived from 10,000 Gaussian simulations. We may wonder if that number of simulations is enough to achieve the convergence. The condition number, defined here as the ratio between the maximum and minimum eigenvalues (see right panel of Fig. 1) is $Cond(C) \sim 10^{12}$. An upper limit for the relative errors in the inverse covariance matrix is $Cond(C) \times \epsilon_{mach}$, where ϵ_{mach} is the computer error, $\epsilon_{mach} \sim 10^{-16}$ for double precision. Thus the relative error for the inverse matrix coefficients is $Cond(C) \times \epsilon_{mach} \sim 10^{-4}$ which is almost negligible. We

have also computed the covariance matrix with two independent sets of 5,000 simulations and constrained the best-fitting f_{nl} of the data with these two matrices. The best-fitting f_{nl} value of the data is almost the same for both matrices and it agrees with the result obtained with 10,000 simulations suggesting that the convergence is almost reached with 5,000 simulations.

We impose constraints on f_{nl} through a χ^2 test. We calculate the expected values of the estimators for different f_{nl} cases using a set of 300 non-Gaussian simulations. In Fig. 2 we plot the expected values of the 364 statistics q_r for several f_{nl} cases for the V+W map. We have checked that the estimator is unbiased. We have evaluated the expected values of the estimator using 200 non-Gaussian simulations of the V+W map and analysed the remaining 100 independent non-Gaussian simulations with $f_{nl} = 50$. The result is an average best-fitting f_{nl} value of 50.6.

In Fig. 3 we plot the values of the statistics for the data map and compare them with the expected values for the best-fitting f_{nl} model. Then we perform a χ^2 analysis to find the best-fitting value of f_{nl} for each map. We also analyse Gaussian simulations in order to obtain the frequentist error bars. Table 2 lists the best-fitting f_{nl} values for the V+W, Q, V and W combined maps and the main properties of the histograms of the best-fitting f_{nl} obtained from Gaussian simulations. In the left panel of Fig. 4 we plot the $\chi^2(f_{nl})$ versus f_{nl} for the V+W map, and in the right panel of Fig. 4 we plot the histogram of the best-fitting f_{nl} of 1,000 Gaussian simulations. We have $-12 < f_{nl} < +86$ for V+W, $-52 < f_{nl} < +77$ for Q, $-32 < f_{nl} < +82$ for V and $+6 < f_{nl} < +123$ for W (all at 95% CL). Note that f_{nl} increases as the frequency grows from Q to V and W bands. This suggests the possible presence of foregrounds residuals as they are more important at low frequencies and they add a negative contribution to f_{nl} for the bispectrum estimator (Yadav & Wandelt 2008). To further check if this is also the case for the wavelet estimator, we have also studied the K and Ka bands, where the foreground signal has an important contribution. We have obtained $f_{nl}^K = -497 \pm 42$ and $f_{nl}^{Ka} = -18 \pm 37$. Taking this into account and the values of f_{nl} for the clean and raw Q, V, and W maps (see Tables 2 and 3) we can see that our estimator is sensitive to the presence of foregrounds (biasing the result towards lower values). The sensitivity
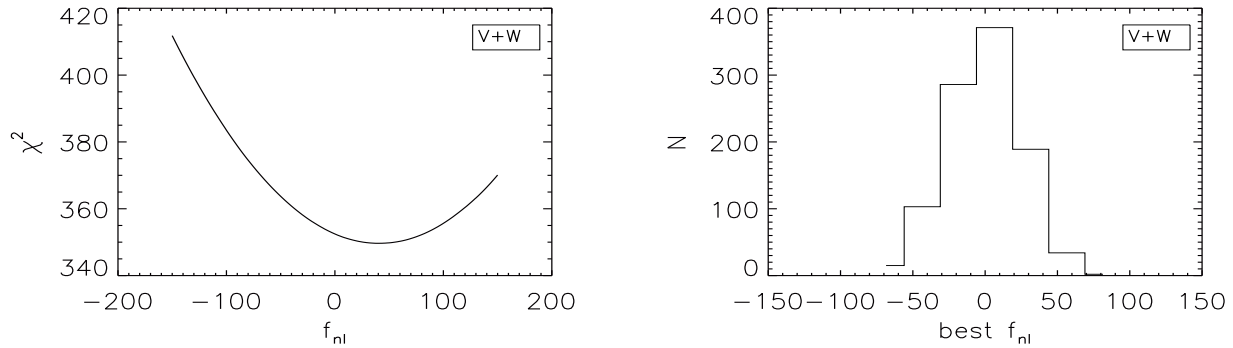
is even more significant for the Q, V, and W bands using the bispectrum (see Table 6 in Komatsu et al. 2009).

It is interesting to point out that the wavelet-based method has an intermediate dimension ($n_{stat} = 364$ for 12 scales) when compared with the bispectrum combinations (ℓ^β_{max} where $2 < \beta < 3$ and $\ell_{max} \sim 10^3$) and the Minkowski functionals (usually several tens of combinations). The number of wavelet cubic combinations increases significantly with the number of scales.

We also estimate the contribution of the point sources for the V+W combined map as in Curto et al. (2009). We add the point source simulations to the CMB plus noise simulations. For each one of them we compute its best-fitting f_{nl} and compare it with the obtained for the same case without including the point source simulation. The difference returns an estimate of the contamination on f_{nl} due to point sources. For the V+W map we have $\Delta f_{nl} = 6 \pm 5$. Therefore our estimate taking into account the point sources is $-18 < f_{nl} < +80$ at 95% CL for the V+W map. Comparing with the best-fitting value for the V+W map given by Yadav & Wandelt (2008), $f_{nl} = 87$, our analysis excludes that value at $\sim$99% CL. However, it is important to point out that Yadav & Wandelt (2008) used different choices for the data maps in the analysis (they used WMAP 3-yr data whereas we use WMAP 5-yr data, different weighting for the channels, etc.), which could also contribute to the found discrepancy. In particular, a simple average of the channels (instead of a noise weighted combination) enhances the signal at high multipoles at the cost of having noisier maps.

3.2. Constraints on f_{nl} with the W band

The W map best-fitting f_{nl} value is only compatible with zero at 99% CL. This result is in apparent discrepancy with the values obtained for the V and V+W maps, which are compatible with zero at 95%CL. The point sources add a low contribution to the W map, $\Delta f_{nl} = 1 \pm 2$, and therefore they do not explain its best-fitting value of $f_{nl} = 65$. We may wonder if that value can be obtained by a statistical fluctuation. Considering simulations with different models ($f_{nl} = 0$, $f_{nl} = 40$ and $f_{nl} = 70$) we have confirmed that the best-fitting f_{nl} for W is compatible with the values obtained for the V and V+W maps.

To understand the relatively large f_{nl} value found in the W map we have performed some additional tests. First of all, we have checked if this deviation could be

due to the presence of residual foregrounds by studying the V-W map for the clean and the raw (before template subtraction) maps as well as the raw maps for the Q,V,W and V+W cases (see Table 3). We find that there is a very significant (positive) deviation in the clean V-W map. Notice that the V-W map has CMB residuals due to the different resolutions of the V and W bands, which have also been taken into account in the V-W simulations. In any case, the signal due to the CMB is very small and we do not expect it to affect the results given in Table 3 for the different maps. Since this combination contains mainly residual foregrounds and noise, both could be responsible for the deviation. Interestingly, when we repeat the test for the raw V-W map, where foreground contamination should be more important, the best f_{nl} value becomes compatible with the simulations. This indicates again that foreground emission tends to bias the estimated f_{nl} towards lower values. This is also observed for the best f_{nl} value estimated for the raw Q, V, W and V+W maps, which is systematically lower than the one obtained for the clean maps. Therefore, for the case of the raw V-W map, some effect from systematics may be cancelled by foreground residuals.

If foregrounds are not responsible for the deviation found in the W and V-W maps, we may wonder if it is due to systematics present in the W radiometers. To test this possibility, we have studied two different combinations of the four W radiometers, where CMB and foregrounds are basically cancelled. One of these combinations is consistent with Gaussian simulations but the second one shows again a deviation at the 95 per cent CL, indicating the possible presence of some spurious signal in the noise of one or several of the W radiometers. In order to localise further the origin of this signal, we have also studied each W radiometer separately, finding a deviation at the level of 98 per cent for the W_2 radiometer, with a best f_{nl} value of 91, while the rest of the radiometers are consistent with the zero value at the 95 per cent CL. Finally we have also considered the difference between the two V radiometers, which is found to be compatible with Gaussianity. This further indicates that, if a systematic is responsible of the V-W map, this would be present in the W frequency channel (see Table 3).

All these tests suggest that the relatively large f_{nl} value obtained for W may come from systematics present

TABLE 3
Best-fitting f_{nl} values for different WMAP radiometers and combinations of them for raw and clean data. We also present the mean and the dispersion of the best-fitting f_{nl} values obtained from Gaussian simulations.

Map	foreground	best f_{nl}	$\langle f_{nl} \rangle$	$\sigma(f_{nl})$
V+W	raw	34	-1	25
Q	raw	-3	0	33
V	raw	16	0	30
W	raw	60	0	30
V-W	raw	-0.02	0.02	0.29
V-W	clean	1.02	0.02	0.29
W_1	clean	39	1	41
W_2	clean	91	-3	45
W_3	clean	23	2	47
W_4	clean	59	0	44
$W_1 + W_2 - W_3 - W_4$	clean	-0.52	0.00	0.34
$W_1 - W_2 + W_3 - W_4$	clean	0.85	0.00	0.35
$V_1 - V_2$	clean	-0.01	0.01	0.34

TABLE 4
Best-fitting f_{nl} values obtained for the northern and southern hemispheres. We also present the mean, dispersion and some percentiles of the distribution of the best fit f_{nl} values obtained from Gaussian simulations.

Region	best f_{nl}	$\langle f_{nl} \rangle$	$\sigma(f_{nl})$	$X_{0.160}$	$X_{0.840}$	$X_{0.025}$	$X_{0.975}$
North	46	2	37	-35	40	-71	74
South	35	-1	38	-39	37	-80	69

possible third order moments (Eq. 2) using appropriate extended masks.

The data are compatible with Gaussian simulations for the considered combined maps (see Table 1). We have imposed constraints on the non-linear coupling parameter f_{nl} by using non-Gaussian simulations with f_{nl}. The results show that f_{nl} increases when we go from the Q to the V and W combined maps. This frequency dependence also appears in the results by Yadav & Wandelt (2008); Komatsu et al. (2009); Curto et al. (2009). The results are compatible with zero at 95% CL for the V+W, Q, and V combined maps, but not for the W map (which is compatible at 99% CL). This value cannot be explained by unresolved point sources since their contribution is $\Delta f_{nl} = 1 \pm 2$ for the W map. We have estimated the probability of having those values with simulations and the results do not show incompatibility among different channels. We have also seen that the relatively large f_{nl} value obtained for the W band may come from systematics in one or several radiometers of this band.

We have also estimated the contribution of unresolved point sources to f_{nl} for the V+W map using a realistic model given by de Zotti et al. (2005). The results are $\Delta f_{nl} = 6 \pm 5$. Taking into account this value, our best estimate for f_{nl} is $-18 < f_{nl} < +80$ at 95% CL. The use of new scales and all the possible third order moments has returned better constrains to f_{nl} and lower error bars compared with the results by Curto et al. (2009) and previous works. Our best estimate is compatible with the values obtained by Komatsu et al. (2009) and it excludes the best-fitting f_{nl} value obtained by Yadav & Wandelt (2008) at the $\sim$99% CL.

Finally we have constrained f_{nl} for the North and South hemispheres and the results give two best-fitting values that are compatible with zero at 95% CL and also are compatible between them. Therefore we do not find any North-South asymmetry for this parameter.

3.3. f_{nl} for the North and South hemispheres

The localization property of the wavelets allows a local analysis of the f_{nl} parameter. In particular, we test the Gaussianity and estimate the best-fitting f_{nl} value of the V+W combined map using only northern (Galactic latitude $b > 0$) and southern pixels ($b < 0$) in Eq. 2. For both cases the third order statistics obtained for the data are compatible with Gaussian simulations (inside the 2σ error bars). In Table 4 we list the best-fitting f_{nl} values for the northern and southern hemispheres and the main properties of the distribution of the best-fitting f_{nl} obtained from 1,000 Gaussian simulations. We estimated the contribution of the unresolved point sources as in the previous subsection, and the values are $\Delta f_{nl} = 7 \pm 7$ for the North and $\Delta f_{nl} = 5 \pm 7$ for the South. Taking into account this, the results are $-32 < f_{nl} < 113$ for the North and $-50 < f_{nl} < 99$ for the South at 95% CL. These values are compatible with zero at 95% CL. We also study the compatibility of the best-fitting value for the North and South hemispheres between them. We compute the difference of the best-fitting f_{nl} value $\Delta f_{nl} = f_{nl}^{(N)} - f_{nl}^{(S)}$ for the North and South hemispheres for the set of 1,000 V+W Gaussian simulations. The difference is $\Delta f_{nl}^{(data)} = 11$ for the data, and for the simulations is $\Delta f_{nl} = 3 \pm 55$. The cumulative probability is $P(\Delta f_{nl} \leq \Delta f_{nl}^{(data)}) = 0.57$ and therefore the difference for the data is compatible with the results obtained from simulations. This means that we do not find any asymmetry in the North-South f_{nl} value.

4. CONCLUSIONS

We have tested the Gaussianity and constrained the f_{nl} parameter with the 5-yr WMAP data. We use an optimal wavelet-based test. We have considered the V+W, Q, V and W combined maps at high resolution. We have used a set of 300 realistic non-Gaussian simulations and thousands of Gaussian simulations for the analysis. We have computed the wavelet coefficient maps at scales from 6.9 arcmin to 500 arcmin and computed all the

in the W radiometers. In any case, a more exhaustive study is necessary in order to establish the origin of this deviation.

REFERENCES

Albrecht, A. & Steinhardt, P. J. 1982, Physical Review Letters, 48, 1220

Bartolo, N., Komatsu, E., Matarrese, S., & Riotto, A. 2004, Phys. Rep., 402, 103

Bennett, C. L., Hill, R. S., Hinshaw, G., Nolta, M. R., Odegard, N., Page, L., Spergel, D. N., Weiland, J. L., Wright, E. L., Halpern, M., Jarosik, N., Kogut, A., Limon, M., Meyer, S. S., Tucker, G. S., & Wollack, E. 2003, ApJS, 148, 97

Cabella, P., Liguori, M., Hansen, F. K., Marinucci, D., Matarrese, S., Moscardini, L., & Vittorio, N. 2005, MNRAS, 358, 684

Cayón, L., Martínez-González, E., Argüeso, F., Banday, A. J., & Górski, K. M. 2003, MNRAS, 339, 1189

Creminelli, P., Nicolis, A., Senatore, L., Tegmark, M., & Zaldarriaga, M. 2006, Journal of Cosmology and Astro-Particle Physics, 5, 4

Creminelli, P., Senatore, L., Zaldarriaga, M., & Tegmark, M. 2007, Journal of Cosmology and Astro-Particle Physics, 3, 5

Curto, A., Aumont, J., Macías-Pérez, J. F., Martínez-González, E., Barreiro, R. B., Santos, D., Désert, F. X., & Tristram, M. 2007, A&A, 474, 23

Curto, A., Macías-Pérez, J. F., Martínez-González, E., Barreiro, R. B., Santos, D., Hansen, F. K., Liguori, M., & Matarrese, S. 2008, A&A, 486, 383

Curto, A., Martínez-González, E., Mukherjee, P., Barreiro, R. B., Hansen, F. K., Liguori, M., & Matarrese, S. 2009, MNRAS, 393, 615

De Troia, G., Ade, P. A. R., Bock, J. J., Bond, J. R., Borrill, J., Boscaleri, A., Cabella, P., Contaldi, C. R., & et al. 2007, ApJL, 670, L73

de Zotti, G., Ricci, R., Mesa, D., Silva, L., Mazzotta, P., Toffolatti, L., & González-Nuevo, J. 2005, A&A, 431, 893

Gangui, A., Lucchin, F., Matarrese, S., & Mollerach, S. 1994, ApJ, 430, 447

Górski, K. M., Hivon, E., Banday, A. J., Wandelt, B. D., Hansen, F. K., Reinecke, M., & Bartelmann, M. 2005, ApJ, 622, 759

Gott, J. R., Colley, W. N., Park, C.-G., Park, C., & Mugnolo, C. 2007, MNRAS, 377, 1668

Guth, A. H. 1981, Phys. Rev. D, 23, 347

Hikage, C., Matsubara, T., Coles, P., Liguori, M., Hansen, F. K., & Matarrese, S. 2008, MNRAS, 389, 1439

Komatsu, E., Dunkley, J., Nolta, M. R., Bennett, C. L., Gold, B., Hinshaw, G., Jarosik, N., Larson, D., Limon, M., Page, L., Spergel, D. N., Halpern, M., Hill, R. S., Kogut, A., Meyer, S. S., Tucker, G. S., Weiland, J. L., Wollack, E., & Wright, E. L. 2009, ApJS, 180, 330

Komatsu, E., Kogut, A., Nolta, M. R., Bennett, C. L., Halpern, M., Hinshaw, G., Jarosik, N., Limon, M., Meyer, S. S., Page, L., Spergel, D. N., Tucker, G. S., Verde, L., Wollack, E., & Wright, E. L. 2003, ApJS, 148, 119

Komatsu, E. & Spergel, D. N. 2001, Phys. Rev. D, 63, 063002

Komatsu, E., Wandelt, B. D., Spergel, D. N., Banday, A. J., & Górski, K. M. 2002, ApJ, 566, 19

Liguori, M., Matarrese, S., & Moscardini, L. 2003, ApJ, 597, 57

Liguori, M., Yadav, A., Hansen, F. K., Komatsu, E., Matarrese, S., & Wandelt, B. 2007, Phys. Rev. D, 76, 105016

Linde, A. D. 1982, Physics Letters B, 108, 389

—. 1983, Physics Letters B, 129, 177

Martínez-González, E. 2008, (arXiv:0805.4157)

Martínez-González, E., Gallegos, J. E., Argüeso, F., Cayón, L., & Sanz, J. L. 2002, MNRAS, 336, 22

Mukherjee, P. & Wang, Y. 2004, ApJ, 613, 51

Pietrobon, D., Cabella, P., Balbi, A., de Gasperis, G., & Vittorio, N. 2009, MNRAS, 396, 1682

Rudjord, Ø., Hansen, F. K., Lan, X., Liguori, M., Marinucci, D., & Matarrese, S. 2009, ApJ, 701, 369

Salopek, D. S. & Bond, J. R. 1990, Phys. Rev. D, 42, 3936

Santos, M. G., Heavens, A., Balbi, A., Borrill, J., Ferreira, P. G., Hanany, S., Jaffe, A. H., Lee, A. T., Rabii, B., Richards, P. L., Smoot, G. F., Stompor, R., Winant, C. D., & Wu, J. H. P. 2003, MNRAS, 341, 623

Slosar, A., Hirata, C., Seljak, U., Ho, S., & Padmanabhan, N. 2008, Journal of Cosmology and Astro-Particle Physics, 8, 31

Smith, K. M., Senatore, L., & Zaldarriaga, M. 2009, Journal of Cosmology and Astro-Particle Physics, 9, 6

Spergel, D. N., Bean, R., Doré, O., Nolta, M. R., Bennett, C. L., Dunkley, J., Hinshaw, G., Jarosik, N., & et al. 2007, ApJS, 170, 377

Verde, L., Wang, L., Heavens, A. F., & Kamionkowski, M. 2000, MNRAS, 313, 141

Vielva, P. & Sanz, J. L. 2009, MNRAS, 397, 837

Yadav, A. P. S. & Wandelt, B. D. 2008, Physical Review Letters, 100, 181301